Monthly Notices
of the
ROYAL ASTRONOMICAL SOCIETY

MNRAS **458,** 1041–1056 (2016)
Advance Access publication 2016 January 29

doi:10.1093/mnras/stw234

Flash ionization signature in coherent cyclotron emission from brown dwarfs

I. Vorgul★ and Ch. Helling

SUPA, School of Physics and Astronomy, University of St Andrews, St Andrews KY16 9SS, UK

Accepted 2016 January 26. Received 2016 January 21; in original form 2015 November 6

ABSTRACT

Brown dwarfs (BDs) form mineral clouds in their atmospheres, where charged particles can produce large-scale discharges in the form of lightning resulting in substantial sudden increase of local ionization. BDs are observed to emit cyclotron radio emission. We show that signatures of strong transient atmospheric ionization events (flash ionization) can be imprinted on a pre-existing radiation. Detection of such flash ionization events will open investigations into the ionization state and atmospheric dynamics. Such events can also result from explosion shock waves, material outbursts or (volcanic) eruptions. We present an analytical model that describes the modulation of a pre-existing electromagnetic radiation by a time-dependent (flash) conductivity that is characteristic for flash ionization events like lightning. Our conductivity model reproduces the conductivity function derived from observations of terrestrial gamma-ray flashes, and is applicable to astrophysical objects with strong temporal variations in the local ionization, as in planetary atmospheres and protoplanetary discs. We show that the field responds with a characteristic flash-shaped pulse to a conductivity flash of intermediate intensity. More powerful ionization events result in smaller variations of the initial radiation, or in its damping. We show that the characteristic damping of the response field for high-power initial radiation carries information about the ionization flash magnitude and duration. The duration of the pulse amplification or the damping is consistently shorter for larger conductivity variations and can be used to evaluate the intensity of the flash ionization. Our work suggests that cyclotron emission could be probe signals for electrification processes inside BD atmosphere.

Key words: instabilities – radiation mechanisms: non-thermal – atmospheric effects – methods: analytical – stars: atmospheres – brown dwarfs.

1 INTRODUCTION

The search for lightning in the Solar system has benefited from an increasing variety of space missions (e.g. *Venus Express*, *Cassini*). Lightning is the most observed flash transient process, that is a powerful but brief, short-term process leading to a local burst of ionization.

Characteristic optical and radio emission provide growing evidence for lightning in Solar system planets (Farrell, Kaiser & Desch 1999; Rakov & Uman 2007). Powerful flash transient processes can act destructively, or they can trigger the formation of new (e.g. pre-biotic) molecules (Miller & Urey 1959). On Earth, lightning is one of the most significant sources of natural ozone production (e.g. Sanghvi 2008). Associated with terrestrial lightning is powerful gamma-ray emission (terrestrial gamma-ray flashes, TGFs;[1] e.g. Fishman et al. 1994; Carlson, Lehtinen & Inan 2010; Dwyer, Smith & Cummer 2012).

We are particularly interested in lighting as an example for flash transient processes in atmospheres of brown dwarfs (BDs) and giant gas planets with respect to observations of cyclotron maser emission that is observed in increasing number of BDs (Hallinan et al. 2007; Yu et al. 2012; Cook, Williams & Berger 2014; Williams, Cook & Berger 2014). BDs have clouds and weather-like variation that determines their dynamic atmospheres (Buenzli et al. 2012; Radigan et al. 2012; Apai et al. 2013; Metchev et al. 2013; Crossfield et al. 2014). Recent *Spitzer* observations suggest the detection of global winds (Heinze et al. 2013). Helling et al. (2013) suggest that in such clouds small-scale spark discharge can be expected at cloud

[1] TGFs are suggested to be produced by runaway electrons, and lightning is suggested to be a source of the electrons' acceleration (Marisaldi et al. 2013; Østgaard et al. 2013).

★E-mail: iv4@st-andrews.ac.uk

bottom, while large-scale discharge should be more common near the top of the cloud or above it. Hence, flash ionization processes can be expected to occur rather frequently in the cloud layers of these ultra-cool objects. Bailey et al. (2013) show that such flash ionization events may affect a larger volume of the atmosphere in BDs than in the atmosphere of Earth.

The observation of cyclotron emission from BDs confirms that strong magnetic fields are present in these ultra-cool objects (Hallinan et al. 2007; Berger et al. 2010; Yu et al. 2012; Burgasser et al. 2013; Cook et al. 2014; Williams et al. 2014). The observation of a strong and coherent cyclotron emission further confirms an existence of a source of ionization to produce the electron beams responsible for the emission.

For hotter stars than M dwarfs and BDs, coronal mass ejections are the sources of accelerated electrons like for example on the radio emitting flare stars like UV Ceti or the magnetic chemically peculiar, extremely fast rotating radio pulsar CU Virginis (Bingham, Cairns & Kellett 2001; Vorgul et al. 2011). The solar wind provides the majority of electrons for planetary cyclotron radio emission (Zarka et al. 2008) for most of the Solar system planets.[2] Most BDs, however, occur as single stars or in BD–BD/ultra-low-mass binary systems. None of the above sources of free electrons is, hence, available to BDs, unless they are part of a binary system where an active M dwarf produces coronal mass ejections or a white dwarf provides high-energy irradiation (Casewell et al. 2015). Cyclotron emission from BDs is powerful and coherent, and the observations of this emission are consistent and reproducible. Possible sources of free electrons leading to strong radio emissions in ultra-cool objects like BDs and free-floating planets are under investigation and include dust–dust collisions (Helling, Jardine & Mokler 2011; Helling et al. 2013), Alfvén ionization (Stark et al. 2013) and cosmic ray impact (Rimmer & Helling 2013). Electric discharges (lightning, transient luminescent events, small-scale but frequent coronal discharges) are additional sources for electrons.

Given that BDs are powerful radio emitters and that clouds and winds form in their atmospheres, we suggest using cyclotron emission as a probe signal (carrier signal) to search for its transformation by atmospheric processes. Recently, Schellart et al. (2015) observed that the lighting radio emission originating from relativistic electrons accelerated in the Earth magnetic field imprint their signal on to the radio signal of cosmic ray-induced atmospheric air showers. In Schellart et al. (2015), the carrier signal for the effect of lighting is the radio emission from a cosmic ray air shower, while a more powerful source is required for the carrier source in the astrophysical context.

Existing data from BDs may already carry the fingerprints of lightning in a form of specific time variations. By studying how a coherent (cyclotron) emission is modulated[3] by flash transient processes, we suggest a new detection method for transient events and for the atmospheres where they occur. We demonstrate how the electromagnetic field of the cyclotron radiation is transformed and how the signatures of the flash ionization are imprinted on to the pre-existing cyclotron emission. *Flash ionization* describes the fast transient events leading to rapid ionization of surrounding medium lightning being one example (Helling et al. 2011). Other discharges include those induced by cosmic rays (Gurevich et al. 1996), explosions, plasma jets or lightning in volcano plumes.

Section 2 contains our approach with details of electron cyclotron emission and a reflection of emission symmetries. The concept of the time-dependent conductivity as a model for lightning is outlined in Section 3. Section 3 presents our mathematical modelling for the electromagnetic field transformed by a flash ionization process represented by a time-dependent conductivity. An exact analytical solution to the equations for a general conductivity function is given in Section 3.2. The temporal variation of the particular flash-like conductivity is modelled in Section 3.3. Section 3.4 presents a test case for our model by comparing the conductivity time variations with TGF observations. The formal body derived in Section 3 is not restricted to radio waves only. Section 4 presents a parameter study that shows how the electromagnetic field responds to different conductivity time flashes. We demonstrate how the amplitude and the damping character changed depending on the strength of the intersected flash ionization event. Section 6 discusses the observational effects of flash ionization events on radio emission from BDs. We summarize this section in a 'Recipe for observations'.

2 APPROACH

This section outlines the approach that we take to derive the signatures of flash ionization events like lighting imprinted on to a pre-existing cyclotron emission. We first summarize necessary facts about electron cyclotron maser (ECM) emission (Section 2.1) and outline our approach to cyclotron emission probing lightning-active regions in Section 2.2.

2.1 Cyclotron emission

Electron cyclotron emission is a localized-source emission, which is known to emerge out of a star/planet's atmosphere shaped as a hollow cone centred around a magnetic pole (e.g. Bingham et al. 2013). Each cone is associated with a distinct source region as indicated in Fig. 1. Such radiation cones form due to a high directivity property of the local cyclotron emission (e.g. Cairns, Vorgul & Bingham 2008), with its annular symmetry reflecting the magnetic field symmetry around the pole. Rotation of the object causes the periodicity of the radiation peaks detected when the cone's walls cross the receiver's line of sight. The width of the observed radiation peaks (e.g. fig. 1 in Hallinan et al. 2008) is determined by the extension of the source and by the path-length along which the radiation propagated and along which it experiences scattering and dispersion effects. It is therefore proportional to the cone wall thickness, Δd, as depicted in Figs 1 and 9.

Cyclotron maser emission occurs when the velocity distribution function of the electron beam, which travels into increasing magnetic field, is continually transformed by magnetic compression to form a horseshoe-shaped distribution in velocity space (Bingham et al. 2001). When eventually the horseshoe is confined enough for the major electron population to satisfy the cyclotron resonance condition, $\omega = \frac{\omega_c}{\gamma} - k_\parallel v_\parallel$ ([4]), the beam emits the cyclotron maser radiation at the location where this resonance happened. Various

[2] Jupiter is slightly offset from the straight line dependence of Solar system planets' radio emission on the solar wind flux, and sources of the accelerated electrons there, including Io volcanic activity, are still debated.

[3] *Modulation of the carrier frequency* refers to the energy transfer between the field and the atmospheric gas that undergoes a flash ionization, and not the field modulation by another radiation field.

[4] where ω_c is a local cyclotron frequency, γ is a relativistic factor, $\gamma = \left(1 - \frac{v_\perp^2 + v_\parallel^2}{c^2}\right)^{-1/2}$, c is the speed of light, and $k_\parallel$ and $v_\parallel$ are wavenumber and particle velocity parallel to the beam direction, respectively.

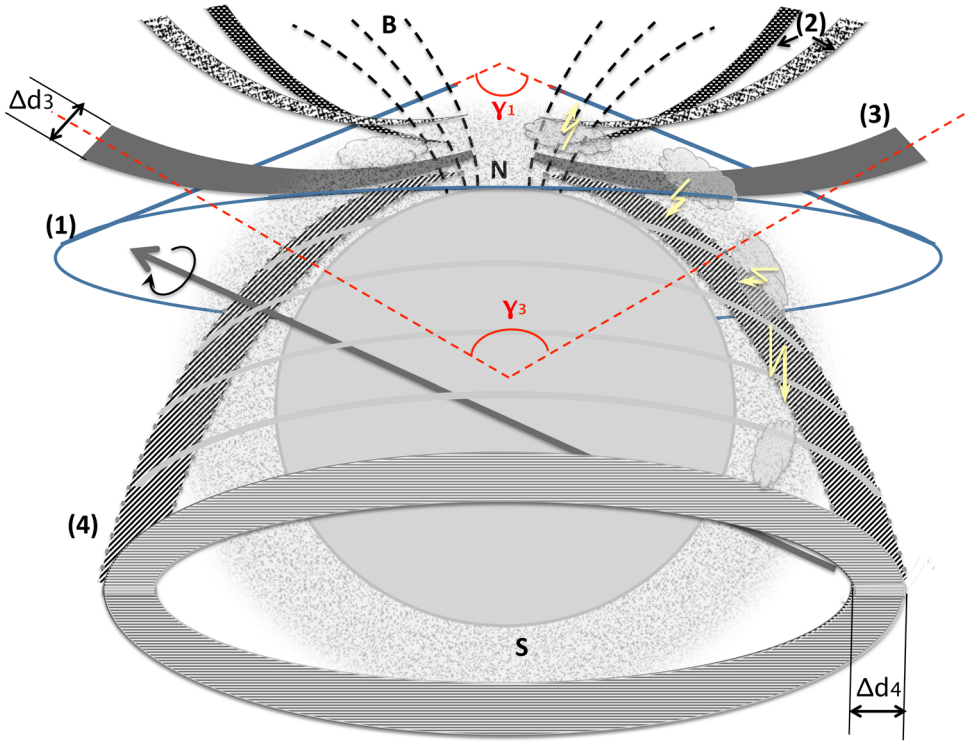

Figure 1. Schematic representation of the radiation cones formed by electron cyclotron emission that originates from a magnetic pole and atmospheric interaction area. Depending on the source area at the magnetic field line near the magnetic pole, the emission cones, (1), . . . ,(4), have different opening angles ($\gamma_1, \ldots, \gamma_4$) and are refracted differently through the atmosphere. The path taken by the radiation will determine the wall thickness ($\Delta d_1, \ldots, \Delta d_4$) with Δd_4 being the thickest of the columns of refracting material passed by the radiation. The magnetic pole (top) does not coincide with the rotational axis.

factors influence the atmospheric altitude at which this resonance occurs, including the initial electron distribution in velocity space, the location where the electrons coupled to the magnetic field, and the magnetic field values, gradient and topology.

It is known from Earth and Saturn direct in-source observations (e.g. Ergun et al. 2000; Lamy et al. 2010) to happen inside plasma cavities with rarefied plasma. This does not imply that the average local density should be low, while higher density can influence the radiation escape. Being emitted from a localized region with small spread along the altitude, the radiation[5] at the source has a sharp frequency spectrum. In addition to the *in situ* observations, this was confirmed by scaled laboratory experiment (McConville et al. 2008). The emission frequency therefore corresponds to the local magnetic field and depends on the altitude at which the emission happened.

The cyclotron radiation is emitted nearly perpendicular to the magnetic field lines (e.g. Mutel, Christopher & Pickett 2008; Speirs et al. 2013), but it can be refracted by the atmospheric gas and clouds before it emerges from the atmosphere in the shape of a hollow cone (Fig. 1). This can also be caused by the non-uniform magnetic field along the path and, consequently, non-uniform plasma frequency and non-uniform refractive index.[6] If the source is far enough from the ionosphere and the radiation is not influenced by propagation effects (case 1 in Fig. 1), the radiation will propagate in a very wide straight cone (almost plane-like, hence γ_1 very close to 180°) with very thin cone walls (opening angles $\gamma_1 \gg \gamma_3$, hence cone wall thickness $\Delta d_1 \ll \Delta d_3$ in Fig. 1). Radio pulsars are examples of the sources of such straight (not refracted) propagation. Typical width of the radio emission cones for pulsars, Δd, is around 2°–8° [e.g. 7.°22, 5.°8 and 4.°2 found in Kramer et al. (1994)]. A summary of the underlying physics and geometry consideration addressing the question why the cyclotron emission appears in hollow cones is given in de Pater & Lissauer (2010). Radio observations from BDs, however, often suggest smaller cone opening angles, γ, and thicker cone walls (>10°), Δd, due to broadened (by propagation) radiation pulses in the observed phase curves. The pulse broadening would be caused by interaction of the emitted radiation with the atmospheric gas and clouds, hence, larger broadening advocating a larger path-lengths (case 3 or 4 in Fig. 1) in contrast to very narrow pulses of non-refracted radiation (case 1 in Fig. 1). Higher frequency cyclotron radiation from the same astrophysical source is emitted deeper into the magnetic field/atmosphere (closer to the magnetic pole where the magnetic field lines converge; see cases 3 and 4 in Fig. 1), and hence it would refract steeper than lower frequency one.

In this case, it is likely to pass through more of the stratified atmospheric volume becoming more affected by the propagation effects, which results in thicker walls of the radiation cones. Note that the effect of different refraction of different frequencies' cones could only be noticeable in observations for a substantial separation of the frequencies to allow for a substantial separation of the local medium properties. With the cyclotron frequency proportional to the local magnetic field ($\nu_e = eB/(2\pi m_e c)$), which decreases from

[5] from a consistent and parameter-stable beam.

[6] Refractive index of plasma in the presence of magnetic field depends on plasma frequency and on the magnetic field, in particular on the angle between the wave vector and the local magnetic field, and is anisotropic in general case. When the magnetic field has its direction and magnitude changing along the wave propagation path, the refractive index for this wave will be inhomogeneous.

the star/planet's surface as $\frac{1}{R^3}$ (R being a radial distance from the object's magnetic dipole centre), the square of the refractive index determined as $n^2 = 1 - \frac{\nu_p}{\nu(\nu \pm \nu_e)}$ (where ν_p is the local plasma frequency and ν is the frequency of the radiation) will also have roughly $\frac{1}{R^3}$ dependence. Therefore, the difference between n^2 at different locations along the magnetic field lines would be proportional to $\frac{1}{R_1^3} - \frac{1}{(R_1+\Delta R)^3} \approx 3\frac{\Delta R}{R_1^4}$, which means that the relative difference in refraction index, $\frac{\Delta n^2}{n_1^2}$, is $3\frac{\Delta R}{R_1}$ times smaller than the correspondent relative frequencies difference, $\frac{\Delta \nu_e}{\nu_{e1}}$.

The effect of two well-separated (in frequencies) cones refracting differently on their way out of the star's magnetosphere is significant in observations from CU Virginis. The effect of refraction was suggested as an explanation for multi-frequency observations to explain why CU Virginis radio observations (e.g. Kellett et al. 2007; Trigilio et al. 2008) found a higher frequency cone (i.e. radiated deeper into the magnetic field and the atmosphere, at lower altitude) inside a lower frequency one, radiated at higher latitude (Lo et al. 2012). The clearly seen refraction there resulted in the cones' walls, Δd, broadening up to 13.°80 and 14.°48 (Kellett et al. 2007).

The idea of cyclotron emission radiated in the shape of hollow cones was applied by Wang & Carr (1995) to derive an opening angle of $\gamma = 80^\circ$ and a cone wall thickness $\Delta d = 15^\circ$ for Neptune's radio emission, and Imai et al. (2002) apply the concept to Jovian radio emission. Observations by Doyle et al. (2010) for the BD TVLM513 suggest an estimation of the opening angle from their fig. 3 being $\gamma = 0.17 \times 360^\circ = 61.2$, and the observed full width half-height (FWHH) of the radiation peak in the same plot can provide an estimation of the radiation cone wall thickness as $\Delta d = 0.065 \times 360^\circ = 23.4$. Observations by Lynch, Mutel & Güdel (2015) present the phase curve of the emission (their fig. 4) from which the cone wall thickness can be estimated as $\Delta d = 1^\circ - 2^\circ$ ('beam angle' in Lynch et al. 2015). This small Δd may indicate the cyclotron source located rather high in the atmosphere, comparable to case 2 in Fig. 1. Williams et al. (2015) observation for NLTT 33370AB (their figs 3 and 4; rotation period $P = 3.7$ h) could be interpreted as a more complicated scenario with a rather small radiation cone with an opening angle estimated from the phase curve as $\gamma = 35^\circ$ and a wall thickness of $\Delta d = 20^\circ - 23^\circ$. Such wide beams (large Δd) (comparable to the refracted CU Virginis beams while being broader than non-refracted pulsar ones) with a relatively small opening angle (γ) may be represented by case 4 in Fig. 1. We note that the number of cones depends on the magnetic field geometry as demonstrated in Kellett et al. (2007).

2.2 How can cyclotron emission probe an atmosphere with lightning-active regions?

BD atmospheres and similarly cold atmospheres, like those of extrasolar giant gas planets, are made of chemically diverse oxygen-rich, H_2-dominated gases. Clouds form and have a distinct influence on the atmosphere through their opacity and through element depletion. BD atmospheres can also be expected to be dynamic as BDs are fast rotators. Giant gas planets may be close to their host star such that irradiation drives strong winds inside their atmospheres. It is plausible to expect that such dynamic, cloud-forming atmospheres generate lighting activity (Helling et al. 2011, 2013) more intensive than in the Solar system and affecting larger atmospheric volumes (Bailey et al. 2013).

Ultra-cool atmospheres may show different kind of discharges in the form of thunderstorms including inter-cloud and intra-cloud discharges. Transient luminous events (sprites, elves, jets, etc.) are frequently observed on Earth in conjunction with lighting. Sprites and jets are substantially more extended than lighting, and therefore increase the atmospheric volume affected by flash ionization events. These flash ionization events perturb the upper atmosphere and magnetosphere (e.g. Siingh et al. 2008). For a BD with a radius of $\sim 7 \times 10^4$ km and a cyclotron peak's half-width of about $\delta\theta = 2^\circ$ (Hallinan et al. 2007; Kuznetsov et al. 2012), the spread of the beam (Δd in Fig. 1) emerging from the atmosphere is $\Delta d = 2\pi \times 7 \times 10^4$ km $\times$ 2 deg /369 deg = 2444 km. If this radiation beam underwent a 10-fold spatial dispersion (for example case 3 in Fig. 1), the source region near the magnetic pole would have an extension (i.e. the cone's wall thickness) about 244 km across. This horizontal (with respect to the star/planet's surface) extent of a storm between 244 and 2444 km determines the volume of the column of the atmosphere which could be probed by the cyclotron beam. Recent observations from Saturn's storm area indicate that the storm that emerges at the surface alone has a head diameter of $\sim$2000 km. Zhang & Showman (2014) demonstrate how the atmospheric dynamic for BDs produces similar pattern. These rough ideas of the radiation/storm longitudinal extensions suggest them to be reasonably comparable for the storms being able to affect a significant portion of the beam's radiation. We suggest that if the ECM radiation travels through the extended atmosphere of the BD/planet, it may be modulated by conductivity changes in the atmosphere produced by flash ionization and can be proposed to probe the extended atmosphere it travels through.

In the following, we consider a local fragment of the radiation cone at a direction that will rotate into the observer's view. Cyclotron emission is a frequency-resonant phenomenon and can therefore be represented by a harmonic wave. We study how this coherent wave changes after experiencing a flash ionization event affecting a volume it paths through.

3 ANALYTICAL MODEL FOR THE ELECTROMAGNETIC FIELD TRANSFORMATION CAUSED BY TIME-DEPENDENT IONIZATION EVENT

We consider a pre-existing coherent radiation (cyclotron radiation or similar) travelling through an atmosphere environment with flash ionization events (e.g. lighting, sprites, flares). Its coherent character allows us to model this incident electromagnetic field as a harmonic wave. We are interested in how the electromagnetic field of a pre-existing emission is transformed by the flash ionization.

The interaction between an electromagnetic wave and a medium rapidly changing in time is highly non-linear. Current approaches that model radiation, emitted by flash ionization processes, are focused on microscopic modelling of charged particle production (electrons and ions; e.g. Carlson, Lehtinen & Inan 2010; Tsalkou, Tikhomirov & Marozava 2013), in some cases including electric (Luque & Ebert 2013) or magnetic (MacLachlan, Diver & Potts 2009) fields. As a result, microscopic approaches predict linear growth rates of the number density of charged particles, and hence, the linear growth stage of electromagnetic emission only. In order to determine the maximum of the flash ionization event, its decline and duration, the non-linear saturation and the consequent drop in the particle velocities and production rate need to be taken into account. This will allow us to qualify and quantify the electromagnetic field response. In the case of an external field probing the flash ionization area, non-linear interactions between field and the transient, ionized medium can be expected to be stronger compared to the discharge's own radiation field because of the higher amplitude

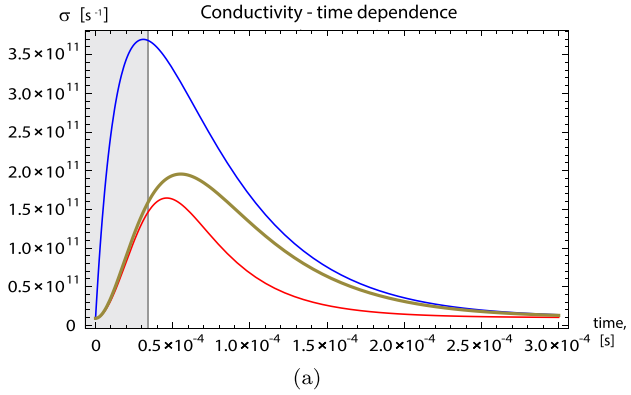

Figure 2. Varieties of conductivity time-dependent shapes, described by the model in equation (20): (a) medium amplitude of the conductivity variation: capacitor-like discharge (blue line) and runaway-initiated breakdown, representing discharges triggered by cosmic rays (red and brown lines); (b) small variations of conductivity within 10 per cent of its initial (background) value. Examples for parameters are given in Table 1. Shaded regions correspond to the duration of the field response, which is a fraction of the conductivity flash's duration.

of the initial (cyclotron) field. We therefore apply the concept of a parametrized time-dependent conductivity in a macroscopic model to allow us to account for non-linear interactions between the ionized medium and the field. We use Maxwell's equations formalism to study the field transformation by the transient processes. We model the flash ionization by a time-dependent conductivity with a flash-like shape. A flash-shape-like conductivity function first rises describing the fast linear growth of the ionized particles at a breakdown ionization stage, then reaching saturation and eventually declines describing the ending of the ionization process (see Fig. 2). This time-dependent functional form is inspired by experimental and observational results (e.g. Gardner et al. 1984; Aleksandrov & Bazelyan 1999; Farrell et al. 1999; Lu et al. 2011). Flash ionization events like lightning, coronal discharges, energetic explosions or eruptions can be suitably described by a time-dependent conductivity without expensive small-scale modelling, because suitable variation in amplitude, duration, shape and the flash front's gradient can be adopted. Conductivity shapes derived from TGFs are a particular well-studied case which we use as test case in Section 3.4.

In Section 3.1, the changing electric field component from Maxwell's equations for a time-dependent conductivity flash is derived, and the exact solution of the derived equations (equations 7–9) is presented in Section 3.2. The time-dependent conductivity function is discussed in Section 3.3 and its relevance of natural discharges in Section 3.4.

3.1 Deriving the equation for the electric component of the electromagnetic field

The electromagnetic fields, $\boldsymbol{E}(t, \boldsymbol{r})$ and $\boldsymbol{H}(t, \boldsymbol{r})$, that interact with a fast-changing medium influence the medium parameters (i.e. dielectric permittivity or conductivity), and these induced changes feed back into the fields. In the model presented in this paper, the electromagnetic fields in a transient medium are described by the linear Maxwell's equations. However, the material coefficients, dielectric permittivity, magnetic permeability or conductivity as part of Maxwell's equations in turn depend on the fields, and therefore the field equations are intrinsically non-linear. This section presents the derivation of the equations for the electric component of the electromagnetic field for a time-dependent conductivity. The interaction of the pre-existing coherent radiation field with the transient event starts at the time $t = 0$. At this moment, the medium's conductivity begins changing in time in a flash-like manner due to the ionization process.

We consider the problem in one spatial dimension, x, and assume that the electromagnetic fields only have components which are perpendicular to that dimension,

$$\boldsymbol{E}(t, \boldsymbol{r}) \equiv E_z(t, x) \equiv E(t, x),$$
$$\boldsymbol{H}(t, \boldsymbol{r}) \equiv H_y(t, x) \equiv H(t, x). \tag{1a}$$

The fields should satisfy Maxwell's equations (in CGS units),

$$\begin{cases} \nabla \times \boldsymbol{E} = -\frac{1}{c}\frac{\partial \boldsymbol{H}}{\partial t}, \\ \nabla \times \boldsymbol{H} = \frac{4\pi\sigma(t)}{c}\boldsymbol{E} + \frac{\varepsilon}{c}\frac{\partial \boldsymbol{E}}{\partial t}, \end{cases} \tag{1b}$$

where ε is a dielectric permittivity of the medium, which is dimensionless and is considered to be constant in time, c is the velocity of light [cm s^{-1}], σ is the time-dependent conductivity [1/s], and E [statV cm^{-1}] and H [Oe] are the electric and magnetic components of the electromagnetic field, correspondingly. Considering 1D electric and magnetic field components only, as in equation (1), the following equation is derived from the system of two Maxwell's equations for E and H components of the electromagnetic field (equation 1 a), by excluding H and collecting the time-dependent conductivity term in the right-hand side (RHS):

$$\frac{\partial^2}{\partial x^2}E(t, x) + \frac{\varepsilon}{c^2}\frac{\partial^2}{\partial t^2}E(t, x) = -\frac{\partial}{\partial t}\left(\frac{4\pi\sigma(t)}{c}E(t, x)\right). \tag{2}$$

The left-hand side of equation (2) is a wave equation for homogeneous media. We assume that the transient processes start at $t = 0$. The left-hand side of equation (2) has a known Green's function (Khizhnyak 1986), which is a solution of a wave equation with the Dirac's delta function $\delta(t - x/v)$ RHS denoting a point source of radiation. Applying convolution of the Green's function to its RHS (Nerukh et al. 2012), the following integral equation for the field results (Vorgul 2007; Cairns et al. 2008)

$$E(t, x) = E_0(t, x)$$
$$-\frac{2\pi}{\varepsilon v}\int_0^{\infty} \mathrm{d}t' \int_{-\infty}^{\infty} \mathrm{d}x' \sigma(t')\,\delta\left(t - t' - \frac{|x - x'|}{v}\right) E(t', x'), \tag{3}$$

where $v = c/\sqrt{\varepsilon}$, and $E_0(t, x)$ is the initial electric component of the field, describing the pre-existing cyclotron radiation (i.e. the field which propagated through the medium before the transient processes start at $t = 0$).

We consider the initial field $E_0(t, x)$ as a plane wave, $E_0(t, x) = E_0 \mathrm{e}^{-\mathrm{i}\omega\left(t - \frac{x}{v}\right)}$, and assume the transformed field's spatial dependence

in the similar form, as

$$E(t,x) = E(t)\mathrm{e}^{\mathrm{i}\omega\frac{x}{v}}. \quad (4)$$

Equation (3) can then be reduced to the following equation for the field's time dependence $E(t)$, after integrating equation (3) over x,

$$E(t) = E_0\mathrm{e}^{\mathrm{i}\omega t} - \frac{4\pi}{\varepsilon}\int_0^t \mathrm{d}t'\sigma(t')\cos\left(\omega(t-t')\right)E(t'). \quad (5)$$

Equation (5) can be transformed after double integration into a second-order differential equation for the field's time dependence, $E(t)$,

$$\frac{\mathrm{d}^2E(t)}{\mathrm{d}t^2} + \frac{4\pi\sigma(t)}{\varepsilon}\frac{\mathrm{d}E(t)}{\mathrm{d}t} + \left(\omega^2 + \frac{4\pi}{\varepsilon}\frac{\mathrm{d}\sigma(t)}{\mathrm{d}t}\right)E(t) = 0. \quad (6)$$

This is a linear differential equation, which accounts for non-linear effects of the flash ionization in Maxwell's equations, equation (1 a), by introducing the time-dependent conductivity, $\sigma(t)$.

Substituting t with a dimensionless τ by $t \to \tau = \omega t$, equation (6) takes a dimensionless form with respect to a normalized electric field, $E_1(\tau) = E(\tau)/E_0$,

$$\frac{\mathrm{d}^2E_1(\tau)}{\mathrm{d}\tau^2} + f(\tau)\frac{\mathrm{d}E_1(\tau)}{\mathrm{d}\tau} + \left(1 + \frac{\mathrm{d}f(\tau)}{\mathrm{d}\tau}\right)E_1(\tau) = 0, \quad (7)$$

where the function f represents the conductivity time dependence,

$$f(\tau) = \frac{4\pi\sigma(t)}{\varepsilon\omega}. \quad (8)$$

The initial conditions for $\tau = 0$ are

$$E_1(0) = 1,$$
$$\left.\frac{\mathrm{d}E_1(t)}{\mathrm{d}t}\right|_{t=0} = \mathrm{i} - \frac{4\pi\sigma(0)}{\varepsilon\omega}. \quad (9)$$

Note that the differential equation (7) could be derived without using the Green's function and integral equation for the field, but using the integral equation allows finding the right initial condition for the field's first derivative, equation (9).

3.2 Solution for the electric field component

We seek to solve equations (7)–(9) to study how an electromagnetic field in an initial form of a harmonic wave can be transformed by transient events. We aim to derive a signature of transients (like lightning) in a pre-radiated field such as coherent cyclotron radiation.

For that purpose, we first reduce the equation (7) to a first-order Riccati differential equation, by substituting the field's time dependence, $E(\tau)$,

$$E_1(\tau) = \mathrm{e}^{\int(u(\tau)-f(\tau)/2)\,\mathrm{d}\tau}. \quad (10)$$

The resulting Riccati equation for the function $u(\tau)$ is

$$\frac{\mathrm{d}u(\tau)}{\mathrm{d}\tau} + u^2(\tau) = -\frac{1}{2}\frac{\mathrm{d}f(\tau)}{\mathrm{d}\tau} + \left(\frac{f(\tau)}{2}\right)^2 - 1, \quad (11)$$

assuming that $f(\tau)$ is known according to equation (8). There are no known solutions for such an equation in general.

We tested various representations of the functions $u(\tau)$ and $f(\tau)$, i.e. different representation of the electromagnetic field and the time-dependent conductivities, $E(\tau)$ and $\sigma(\tau)$. We found that if the function $f(\tau)$ is expressed through a function $b(\tau)$, such that

$$f(\tau) = Cb(\tau) + \frac{1}{b(\tau)}\frac{\mathrm{d}b(\tau)}{\mathrm{d}\tau} - b(\tau)\int\frac{\mathrm{d}\tau}{b(\tau)} \quad (12)$$

(C is an arbitrary constant), an exact particular solution to the Riccati equation (11) can be written as

$$u(\tau) = \frac{C}{2}b(\tau) - \frac{1}{2b(\tau)}\frac{\mathrm{d}b(\tau)}{\mathrm{d}\tau} - \frac{b(\tau)}{2}\int\frac{\mathrm{d}\tau}{b(\tau)}. \quad (13)$$

The representation of the conductivity function $f(\tau)$ in terms of another function $b(\tau)$ in equation (12) is just a substitution of one function with another, in order to get mathematical advantages. It is valid for any function and does not involve any assumptions on the functions. The resulting Riccati equations (11) and (13) are therefore exact equivalents of the wave equation (7) for the electric component of electromagnetic field.

A particular solution for the electromagnetic field determined by equation (10) is then

$$E_{\mathrm{part}}(\tau) = \mathrm{e}^{\int(u(\tau)-f(\tau)/2)\mathrm{d}\tau} = \mathrm{e}^{\int\left(-\frac{1}{b(\tau)}\frac{\mathrm{d}b(\tau)}{\mathrm{d}\tau}\right)\mathrm{d}\tau} = \frac{1}{b(\tau)}. \quad (14)$$

To find a general solution for the electromagnetic field, the substitution (in terms of a new introduced function $z(x)$)

$$E_1(\tau) = E_{\mathrm{part}}(\tau)\cdot z(\tau) = \frac{z(\tau)}{b(\tau)} \quad (15)$$

transforms the initial differential equation (7) for the field, with the conductivity-related function $f(\tau)$ expressed as in equation (12), into a first-order ordinary linear differential equation for the derivative of $z(\tau)$,

$$\frac{\mathrm{d}^2z(\tau)}{\mathrm{d}\tau^2} = \frac{\mathrm{d}z(\tau)}{\mathrm{d}\tau}\left\{-Cb(\tau) + \frac{1}{b(\tau)}\frac{\mathrm{d}b(\tau)}{\mathrm{d}\tau} + b(\tau)\int\frac{\mathrm{d}\tau}{b(\tau)}\right\}, \quad (16)$$

which can be solved easily. The solution of equation (16),

$$z(\tau) = C_2 + C_1\int_0^\tau \mathrm{d}\tau\,\mathrm{e}^{\int\left(-Cb(\tau)+\frac{1}{b(\tau)}\frac{\mathrm{d}b(\tau)}{\mathrm{d}\tau}+b(\tau)\int\frac{\mathrm{d}\tau}{b(\tau)}\right)},$$

gives the following general solution for the time-dependent electromagnetic field:

$$E_1(\tau) = \frac{C_2}{b(\tau)} + \frac{C_1}{b(\tau)}\int_0^\tau \mathrm{d}\tau\,b(\tau)\mathrm{e}^{\int\left(-Cb(\tau)+b(\tau)\int\frac{\mathrm{d}\tau}{b(\tau)}\right)}. \quad (17)$$

The constants C_1 and C_2 are found from the initial conditions in equation (9) to be

$$C_1 = \left(i - Cb(0) + b(0)\left.\int\frac{\mathrm{d}\tau}{b(\tau)}\right|_{\tau=0}\right)\mathrm{e}^{-\left\{\int\mathrm{d}\tau\left(-Cb(\tau)+b(\tau)\int\frac{\mathrm{d}\tau}{b(\tau)}\right)\right\}\Big|_{\tau=0}},$$
$$C_2 = b(0). \quad (18)$$

The solution for the field (equation 17) is an *exact general solution* describing how the radiation field is transformed by time variations of conductivity as described in a general form by equation (12). Advantages of exact analytical solution over numerical solutions are much more profound for powerful fast processes (i.e. mathematically, for large-amplitude rapidly varying coefficients of differential equations at a time-scale comparable to the wave period), as conventional numerical techniques fail to produce correct reliable results in this case. We are interested in the case when the conductivity's time dependence has a flash-like shape, describing localized ionization or discharge events. We demonstrate in Section 3.3 how we model the time-dependent conductivity by the choice of a function $b(\tau)$ that describes a flash-like ionization event.

3.3 Conductivity time dependence for flash ionization processes

The function $b(\tau)$ determines the time dependence of the conductivity by equation (12), as well as the solution for the electromagnetic field by equation (18). We wish to describe the conductivity flash variation most accurately by allowing it to be as flexible as possible. We require our model to be able to describe two different types of lightning discharges: a capacitor-like one and one induced by runaway electrons. A time dependence corresponding to a runaway-induced discharge, like that known for cosmic ray-induced lightning discharges (Gurevich & Karashtin 2013), starts as exponential growth. Unlike a capacitor-like discharge, which would start with almost linear growth and requires a high degree of charge separation, runaway discharges require less initial potential difference (see e.g. Helling et al. 2013). The runaway-initiated discharges are therefore more easy to start, subject to existence of a small population of runaway electrons. The time-dependent conductivity of such initiated discharges starts as an exponential growth of the conductivity due to the breakdown of the avalanche.

We represent the time-dependent conductivity by the function $b(\tau)$ which allows us to describe both the capacity and the runaway breakdown discharges as part of the same formulae:

$$b(\tau) = \frac{(\tau^k + B)^2 \mathrm{e}^{b\tau}}{A\left(\tau^{2k} + (D+B)\tau^k + k(D-B)\tau^{k-1} + BD\right)}. \tag{19}$$

The conductivity changing with time from equation (11) is now

$$f(\tau) = \frac{A(\tau^k + D)\mathrm{e}^{-b\tau}}{(\tau^k + B)} + C. \tag{20}$$

The parameters A, B, C, D, b and k are used to describe the desired variety of the particular time dependence's shape. Fig. 2 demonstrates various cases of the time evolution of the flash-like conductivity that we are interested in. The blue line in Fig. 2(a) shows a capacitor-like discharge, while two other curves demonstrate a runaway-initiated discharge (like one triggered by cosmic rays). Fig. 2(a) shows *intermediate*-value conductivity flashes, while Fig. 2(b) shows small variations of conductivity within 10 per cent of the background value, i.e. the value existing there before the flash ionization event (e.g. background thermal ionization in BDs). Equation (20) allows for the analytical solution of the problem of electromagnetic field transformation, while describing the desired features of the conductivity variations. The general solution for the electric field component is then described by equation (18) with the function $b(\tau)$ as given in equation (19).

This general solution for the electric field component describes a pre-existing radiation's response to a flash ionization event. Such events can take place in cloudy substellar atmospheres but also in, for example, protoplanetary discs.

3.4 Form of conductivity time variations as a result of natural discharges

Time-dependent conductivity corresponding to a flash ionization process could be expected in a form of a flash-like shape, first rising due to fast growth of the ionized particles at a breakdown ionization stage, then reaching saturation and eventually declining when the process is over. Direct and indirect (through measuring a current) evidence of a flash-shape time-dependent conductivity can be found in observations [e.g. on Earth (Lu et al. 2010) or on Jupiter (Farrell et al. 1999)] and experiments [e.g. nuclear lightning (Gardner et al. 1984) or laboratory experiment (Aleksandrov & Bazelyan 1999)].

To check the relevance of our conductivity flash model to lightning discharges and similar phenomena and to conclude on quantitative parameters which can be expected for the conductivity flash, we look into the observational results of a discharge associated with TGF analysed in Lu et al. (2011). Detection of radio signals in ultra-low frequencies (ULF) and very-low frequency (VLF) was reported, with gamma-rays detected within 0.2 ms of the fast discharge. Similar distinctive variations of the waveforms were reported for another TGF-associated intra-cloud discharge (Lu et al. 2010). TGF production was reported to be associated with the upward-propagating leader during the initial development of compact (1.5–2 km channel) intra-cloud flash within 30 km of the sub-satellite point.

We use the integral Ohm's law

$$j(t) = \int_0^t \sigma(t - t')E(t')\mathrm{d}t' \tag{21}$$

to retrieve the conductivity variation in time, corresponding to currents and fields which resemble the observed waveforms (Lu et al. 2010, 2011). $j(t)$ and $E(t)$ in equation (21) are the electrons current and electric field, correspondingly.

The current and the field have a flash-like pulse waveforms in observations for the events like lightning discharges or TGFs. Often, this form is modelled with double-exponential representation (Farrell et al. 1999). We use the representation

$$\begin{cases} j(t) = j_0(t - t_0)^n \cdot \mathrm{e}^{-\alpha t} + c, \\ E(t) = E_0(t - t_0)^m \cdot \mathrm{e}^{-\beta t} + C \end{cases} \tag{22}$$

for them, which describes the pulse shape reasonably accurate and allows analytical Laplace transforms, while not leading to divergence in inverse Laplace transform, as a double-exponential representation would do. The parameters n, m, α and β as well as the integration constants c and C are determined from reproducing TGF-associated lighting discharge from Lu et al. (2011) in Fig. 3.

For known waveforms of the current and the field, equation (21) becomes an integral equation for the conductivity $\sigma(t)$. The integral Ohm's law reflects the fact that the current and the field are not only affecting each other at any particular moment, but the full pre-history of their time evolution has its influence.

Equation (21) is a Volterra-type integral equation of a convolution type. This allows transforming it into an algebraic equation by Laplace transform, $t \to p$, and deriving then the conductivity as follows:

$$\hat{\sigma}(p) = \frac{\hat{j}(p)}{\hat{E}(p)}. \tag{23}$$

The time-dependent conductivity can be found from equation (23) after applying an inverse Laplace transform,

$$\sigma(t) = \int_{-i\infty+\alpha}^{i\infty+\alpha} \mathrm{e}^{pt} \frac{\hat{j}(p)}{\hat{E}(p)}\,\mathrm{d}p = \int_{-i\infty+\alpha}^{i\infty+\alpha} \mathrm{e}^{pt} \frac{\int_0^\infty j(t')\mathrm{e}^{-pt'}\mathrm{d}t'}{\int_0^\infty E(t')\mathrm{e}^{-pt'}\mathrm{d}t'}\,\mathrm{d}p. \tag{24}$$

The current and the field in equation (24) are determined by equation (22).

We use the current and the field resembling those in Lu et al. (2010, their fig. 3) to retrieve the conductivity waveform (its time dependence). Fig. 3 shows the current (red solid) and the field (blue dashed) and the resulting retrieved conductivities for two cases of different time delays between the field waveform emission and the discharge current. While the shape of the conductivity time variation does not depend on the time delay, its peak value depends

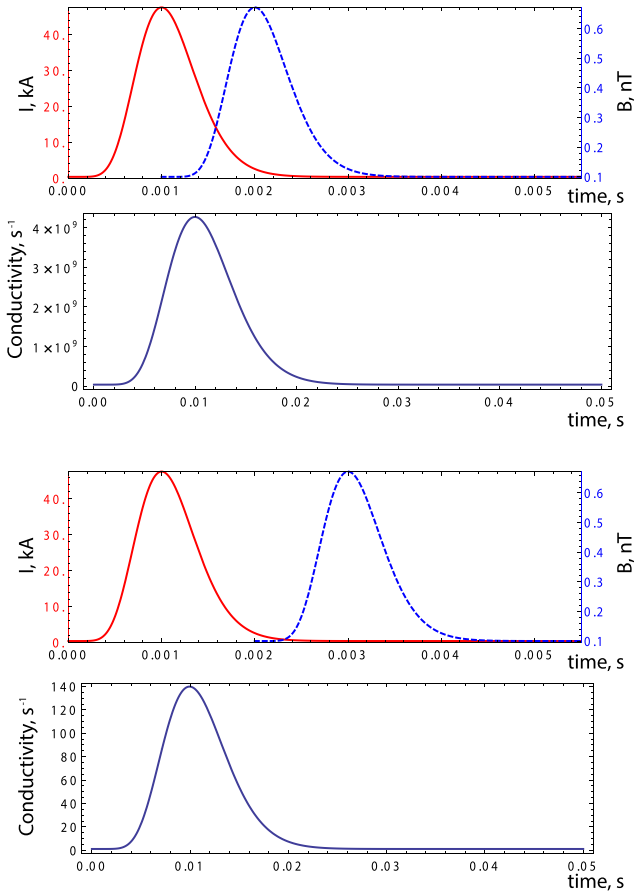

Figure 3. Waveforms of the electric current, I [kA] (red), and of the magnetic component of electromagnetic field, B [nT] (blue), with the retrieved conductivity time dependences [1/s] for the correspondent I and B combinations plotted below them. The electric current and the field have the waveform parameters similar to the observational results for a TGF-associated lightning discharge reported in Lu et al. (2011). Two different plots are for different delays of the electromagnetic production with respect to the current.

on it dramatically. Estimation of the time delay however relies on accuracy of estimations for the distance from the detectors to the discharge and for the correspondent velocities. The duration of the retrieved conductivity flash does not depend on that delay, and is almost 10 times longer than that of the current or field pulses (flashes). Similar results were obtained for the current and field waveform reported in Farrell et al. (1999) for Saturn observations, but the conductivity flash duration is comparatively shorter, being about five times longer than that of the current and the field. Our model described by equations (19) and (20) with conductivity plotted in Fig. 2 is well representative of the flash ionization events like lightning discharges, as comparison with the retrieved conductivity (Fig. 3) suggests.

4 THE IMPRINT OF A TIME-DEPENDENT IONIZATION ON A RADIATION FIELD

Flash ionization events like lightning, coronal discharges, energetic explosions or eruptions can be suitably described by the time-dependent conductivity (equation 20), because this formula allows one to adapt a suitable variation in amplitude, duration, shape and the flash front's gradient. We have demonstrated in Section 3.4 that our model does reproduce the well-studied case of TGFs' current (e.g. Lu et al. 2010, their fig. 3).

We consider the conductivity's temporal variations through flash ionization in a medium with a small value of natural background conductivity, e.g. through thermal ionization (Rodrigues-Barrera et al. 2015). This background ionization is physically required to start the flash ionization. From a mathematical point of view, the background ionization is not necessary, and all the derived formulae remain valid if the initial (background) conductivity is zero. Fig. 2(a) shows larger amplitude changes in conductivity, while Fig. 2(b) demonstrates the changes within a few per cent of the background value.

The purpose of this paper is to study if and how the electric field changes for different flash ionization events (like coronal discharges, lightning or sprites), which we represent by various conductivity profiles (equation 20; Fig. 2). As we aim to find signatures of the flash ionization events in pre-existing cyclotron radiation, we consider radio frequencies as the incident radiation field in our analysis, i.e. as a carrier signal for the modulation imposed by a flash ionization. The analytical results from the previous sections are valid for any frequency, i.e. for any relation between the initial wave frequency and the time-scale of the ionization process, as long as the assumption of a simultaneous conductivity change in different points of the local medium is reasonable.

Using the model formulae presented in Section 3, Fig. 4 demonstrates how the electric field (equation 18) responds to a flash-like pulse due to a fast change of conductivity.

(i) The response of the electric field begins when the conductivity flash has a high positive gradient.
(ii) The maximum of the field response corresponds to the time of the maximum conductivity gradient.
(iii) The field responds on a significantly shorter time-scale than the time-scale of the underlying process responsible for the rapid conductivity change.
(iv) The pulse duration of the response field is typically about 10 times shorter than the conductivity flash duration.

For a fixed duration of the conductivity time flash,[7] the duration of the response field pulse's versus the conductivity peak value is shown in Fig. 6. Remarkably, the field response becomes shorter in time the more powerful the ionization process is (i.e. for a larger peak value of the flash's conductivity).

Fig. 7 demonstrates that the field response also starts slightly later for flashes with larger peak value of conductivity, when making the comparison at the same fixed position of the conductivity maximum. This can be attributed to the fact that the maximum gradient of the flash is reached slightly later for larger flashes. The duration of the responding electric field pulse (Fig. 4) is at least one order of amplitude shorter than the duration of the ionization flash.

Investigating the dependence of the amplitude of the electric field response pulse on the amplitude of the conductivity flash (Fig. 5) shows that for small variations of the conductivity in time [within a few per cent, as shown in Fig. 2(b)] the field's change is not noticeable. For *intermediate* changes in time, however, the response amplitude will be larger for more powerful ionization (larger flash of conductivity, see Fig. 7).

Note that the conductivity can be described as sums of the products of densities for all available charges and the charges'

[7] The duration is taken at the half-height of the pulsed shape.

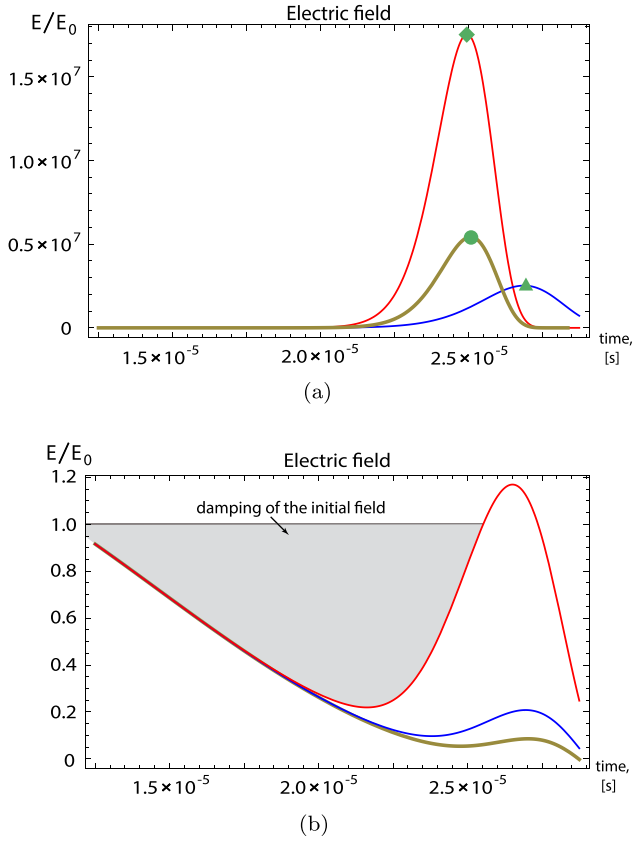

Figure 4. Typical electric field transformation (a) for *intermediate* conductivity flashes; (b) for larger conductivity flashes. Colour code for the field is the same as for the conductivity time dependences shown in Fig. 2. Time interval on the plots corresponds to the grey area in Fig. 2. The *intermediate* conductivity flash results in a characteristic response in a form of a flash-shaped pulse of electric field, which can be substantially amplified with respect to the initial field amplitude (a). The large-amplitude conductivity flashes in time result in smaller field response, and for flash-character damping of the incident field (b).

mobilities,

$$\mu = \frac{v_{\rm drift}}{E_{\rm electrostatic}}, \tag{25}$$

where $v_{\rm drift}$ is the electrons' drift velocity and $E_{\rm electrostatic}$ is the local electrostatic electric field. During the avalanche (breakdown) process, the mobility of electrons as well as their number density is much higher than those of ions or charged dust grains, so we only take electrons motion into account. The conductivity is then determined by

$$\sigma = e\mu_{\rm e}n_{\rm e}, \tag{26}$$

where e is a charge of the electron, $n_{\rm e}$ is electrons' number density and $\mu_{\rm e}$ is the mobility of the electrons. A higher peak value of conductivity requires therefore a combination of strong ionization and charge acceleration.

For larger peak conductivities, the response field peak value becomes less sensitive to the further increase of the conductivity, with the dependence shown in Fig. 5 reaching saturation. Points shown with a triangle, a circle and a diamond in Fig. 5 correspond to the curves marked with the same symbols in Fig. 4(a) and lay within *intermediate* flash ionization intensity. Increasing the peak conductivity even further (considering more powerful flash ionization

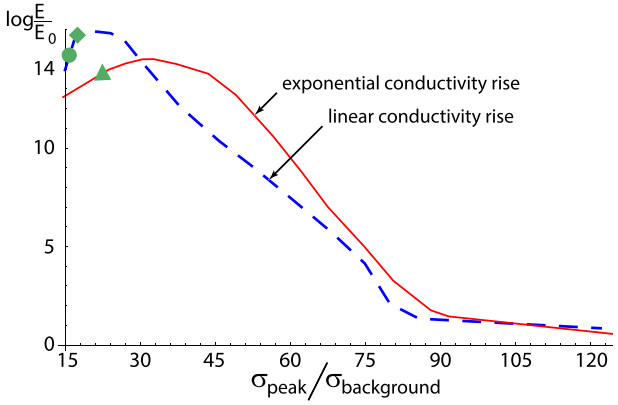

Figure 5. The relative electric field amplitude, $\log(E/E_0)$, at its maximum value, versus the maximum (peak) value of relative conductivity change with respect to the background conductivity, $\sigma_{\rm peak}/\sigma_{\rm background}$. Dashed and solid curves correspond to the cases of conductivity rising linearly up at the beginning of the flash process [corresponding to the blue curve in Fig. 4(a)] and conductivity with exponential growth at the beginning of the flash [corresponding to the red curve in Fig. 4(a)]. One can see that bigger field response does not always correspond to bigger flash of conductivity (i.e. larger peak value of conductivity).

processes) leads to reversal of the effect: the field response becomes smaller for larger conductivity flash, i.e. the normalized field amplitude, E/E_0, decreases with increasing the relative conductivity change ($\sigma_{\rm peak}/\sigma_{\rm background}$).

It is known that lightning discharges radiate an electromagnetic field (e.g. Uman 1964; Farrell et al. 1999; Rycroft 2006; Rakov & Uman 2007). This radiation occurs when runaway electrons, produced by ionizing discharges, form conducting currents which act as radiating antennas. The radiation is produced during the energetic phase of the discharge, when the runaway electrons are still fast enough to radiate,[8] and when their radiation is not yet fully damped by collisional losses. Similarly, the short-term amplification of the pre-existing radiation in a flash-ionized medium, as seen in Fig. 4(a), is caused by contributions of the energetic electrons' radiative currents. Both mobility and charges number density influence conductivity, as seen in equation (26). As noted in Section 1, the conductivity in our model[9] is a combination of all effects from ionization and charges movement, including the reactive and the dissipative responses. The peak of the field amplification corresponds roughly to the maximum gradient of the rising conductivity. This reflects on the dynamics between two mechanisms of rising conductivity: the one associated with increasing charges mobility and the one associated with increasing number density of charges. Runaway breakdown at the first stage of the discharge dramatically increases the charge mobility aspect of the conductivity, while consequent continuing increase in conductivity is caused mostly by the increased number of charges from collisional ionization. This second stage of the conductivity rise will effectively damp the produced radiation/amplification.[10]

[8] Mechanism of radiation here similar to radiation from an electric current.
[9] which is a general model for a transient electromagnetics as derived from Maxwell's equations.
[10] Ionizing discharges' ability to produce a short-term field amplification is known and utilized in laboratory (e.g. Bickerton 1958; Skordoulis et al. 1990).

While one might intuitively expect that a more powerful ionization process would lead to a higher response in the electromagnetic field's amplitude, our results show that there is some threshold in the peak value of conductivity (which is different for different initial conditions and shapes of the conductivity time flashes), corresponding to the peaks, after which (i.e. for the conductivity change bigger than that value) the field response decreases for larger flashes. The reason for this is that, above a certain threshold, the conductive medium would be efficiently damping the field, allowing the damping to prevail over the effect of pumping the field by the transient event's energy. An ionized medium (like the ionosphere) is generally non-transparent to most of the radio frequencies. This is one of the biggest problems with observing lightning discharges from outside of the Solar system or terrestrial planets. With additional energy coming into the radiation field from powerful ionization processes, such a field has a chance to penetrate through even an initially ionized medium. However, processes of higher extremity (involving larger peak value of conductivity flash) would result in a metal-like ionized area which would damp the electromagnetic field dramatically. The classification is based on the effect which is produced by the transient event on the electromagnetic field, e.g. 'strong' event ('big' conductivity flash) attributes to damping the field, as in Fig. 4(b), while 'intermediate' event denotes the flash resulting in the field amplification, as in Fig. 4(a). Small events (i.e. the ionization events which change the conductivity within a few per cent of its initial value) do not produce noticeable signatures.

The field's response amplitude cannot therefore be used as a single criterion for the power of the underlying ionization process, and most powerful flash ionization processes (including, for example, discharges/lightning and explosions/eruptions) can be missed by observations. The duration of the electric field response pulse, however, provides the information about the magnitude of the conductivity flash, as it universally decreases with the increasing conductivity flash amplitude for the same fixed duration of the conductivity flash.

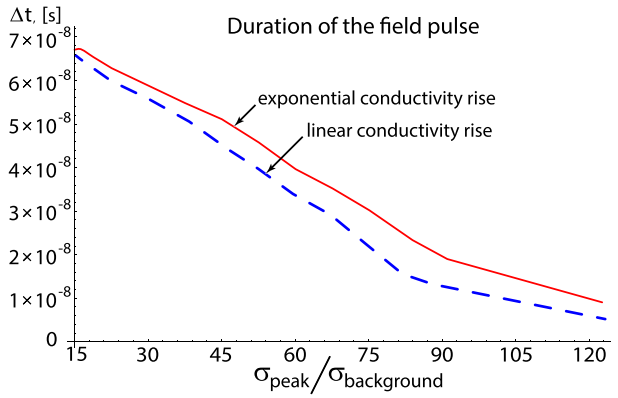

Figure 6. Dependence of the electric field pulse duration on maximum value of relative conductivity change with respect to the background conductivity, $\sigma_{\rm peak}/\sigma_{\rm background}$. The duration is measured at 1/2 of the field's maximum value at its peak. Colour code is the same as in Fig. 5. The response field pulse is consistently shorter for larger flash of conductivity (larger peak conductivity value).

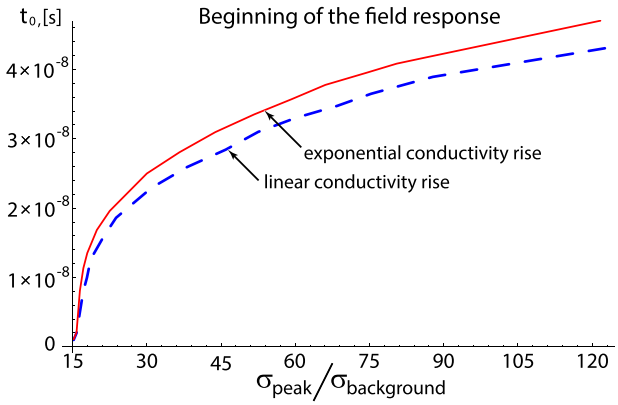

Figure 7. Dependence of the electric field pulse start time, t_0, on maximum value of relative conductivity change with respect to the background conductivity, $\sigma_{\rm peak}/\sigma_{\rm background}$. The start time is determined on the field-rising slope at 1/2 of the field's maximum value at its peak. Colour code is the same as in Fig. 5. The field response starts consistently later for larger flash of conductivity (larger peak conductivity value).

5 OBSERVATIONAL EFFECTS OF FLASH IONIZATION ON RADIO SIGNALS FROM A BD

5.1 Frequency of the radiation

We apply our model to the case of radio wavelength being the pre-existing signal that can be modulated by a flash ionization event. Our choice of parameters is guided by observations of cyclotron radio emission from BDs and late M dwarfs. 4.8 GHz frequency observations were reported from a late M dwarf (Burgasser et al. 2013), and observations of radio emission from BDs in the frequency range 4.4–4.9 GHz were presented in Route (2013). Hallinan et al. (2007) also observed cyclotron emission from BDs at 4.88 and 8.44 GHz, and radio emission at 5.8 GHz was reported by Williams et al. (2014). The radiation frequency, being related to local cyclotron frequency of electrons, is proportional to local magnetic field. BDs' and other ultra-cold dwarfs (UCDs') magnetic field is of the order of a few kG (Schrijver 2009), providing the cyclotron radiation frequency of order of a few GHz. A few gauss planetary magnetic field results in a cyclotron radio emission in tens kHz to few MHz frequency range [e.g. de Pater & Lissauer (2010) for Jupiter].

All our typical results are shown for $\omega = 4.8 \times 10^9$ rad s^{-1} (cyclic frequency) in Figs 4–7. They are representative for other frequencies as well, as we demonstrate by Fig. 8 for the alternative incident radiation frequency $f = \omega/2\pi = 1.59$ MHz.[11] The transformed electric field given by equations (17)–(18) does not scale with the frequency exactly. However, within the radio frequency range, the temporal characteristics of the field (start time and duration of the response, Figs 6 and 7) still roughly scale with the frequency as ω^{-1}, which makes our analysis more general.

5.2 Peak value of conductivity

Another key input value for the model of the flash is a peak value of conductivity. We showed in Section 3.4 that the peak conductivity corresponding to terrestrial TGFs can be expected within a wide range of values, depending on an actual delay time between the measured current and field. For a cloud-to-ground discharge on Earth, the peak value of temporal variation of the local temperature $T_{\rm gas}$ is typically about $T \sim 24\,000$ K (Uman 1964). A value

[11] Similar magnitude of the transformed field is achieved for about 500 times higher peak value of conductivity at the flash.

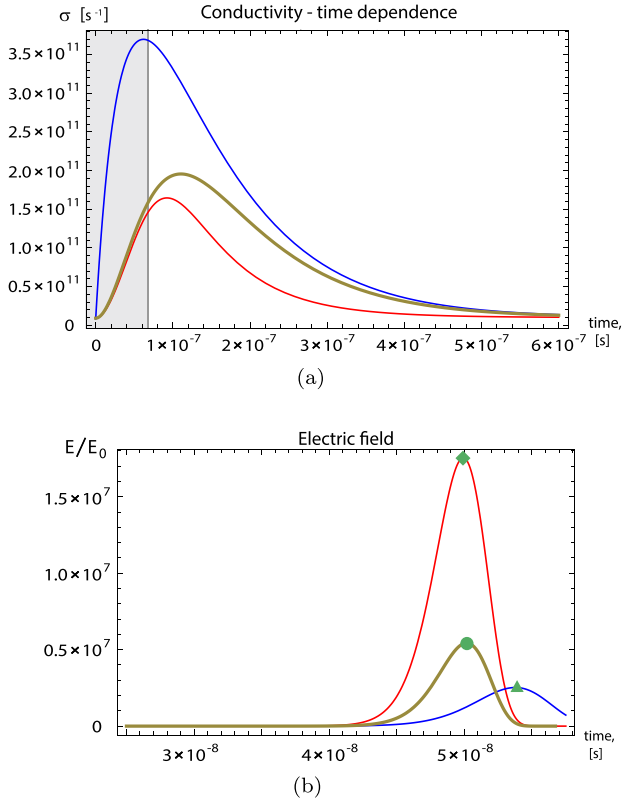

Figure 8. (a) Conductivity time dependence and (b) electric component of the electromagnetic field transformation for the frequency of initial radiation $f = 1.59$ MHz.

for the conductivity derived by these authors was calculated to be $\sigma \approx 1.08 \times 10^9$ s^{-1}.[12] This is the conductivity that can be expected within an active lightning channel on Earth. For the surrounding area, where the lightning would produce flash ionization of some (sometimes substantial) volume, the conductivity is smaller than in the channel, which could correspond to both 'big' and 'intermediate' flash regimes (as defined in Section 6). However, there are no values for the peak conductivity for those areas in the literature. Only the 'intermediate' flash effects can be seen by short-time amplification as in Fig. 4(a). However, the damping of the field as shown in Fig. 4(b) can also serve as an indication of an atmospheric flash, though high-intensity initial (cyclotron) radiation or high signal resolution, sufficient for detecting 30–60 per cent variations in amplitude [such degree of damping of the initial field is suggested by Fig. 4(b)], is required.

The conductivity of a medium can be calculated using equation (26). Runaway electrons from the channel ionize the surrounding medium. The conductivity is then proportional to the electron drift velocity, $v_{\rm drift}$. The velocity, and therefore the mobility, is exponentially decaying with time (Bruce & Golde 1941) after the short initial period of electrons' acceleration by the ionization flash,

$$\mu_{\rm e} \sim v(t) \sim {\rm e}^{-\gamma t}.$$

[12] Found in Uman (1964) conductivity is converted into CGS units as

$$\sigma \approx 180 \times 10^{-2}\ \Omega^{-1}\,{\rm m}^{-1}({\rm SI\ units}) = 180 \times 10^{-2} \times 9 \times 10^9\ {\rm s}^{-1} = 1.08 \times 10^9\ {\rm s}^{-1}. \quad (27)$$

The number density of electrons is growing exponentially at runaway breakdown before it reaches a saturation at about or after the moment when the electrons start slowing down, $n_{\rm e} \sim {\rm e}^{\beta t}$. A product of these two exponents, as in equation (26), one of which is time-shifted (with the decay starting with some initial time delay) and another is growing till the moment of saturation, results in the flash time dependence of conductivity. According to Rakov & Uman (2003), the 'burning point' at lightning discharge moves at 10^5 km s^{-1}, while the tip velocity of sprites from microdischarge model is 10^4 km s^{-1} (Rycroft 2006). Exponential decay in the runaway electrons velocity (Bruce & Golde 1941) would result in an average peak conductivity across the transient region of about $\sigma_{\rm peak} \sim 10^4$ s^{-1}. The $\sim 10^{-5}$ s duration of the conductivity flashes was considered above as this would be within average values for the duration of a cloud-to-ground discharge on Earth. The peak conductivity of 10^4 s^{-1} corresponding to this duration is small enough to be classified as an 'intermediate' flash which amplifies the field, as Fig. 4(a) suggests.

With high-pressure atmospheres like those of BDs the number of branches in lightning trees grows significantly with increasing pressure (Briels, Veldhuizen & van and Ebert 2008; Bailey et al. 2013). This makes our model of a homogeneous time-dependent conductivity more easily applicable to atmospheres of BDs. Lightning on other planets and on BDs can be more powerful and longer in time than on Earth, see e.g. Farrell et al. (2007). The duration of the flash ionization of the area surrounding the lightning channel can also be expected to be longer than the lightning flash itself. For longer conductivity flash, the peak conductivity as $\sigma_{\rm peak} \sim 10^4$ s^{-1} would still be within 'intermediate' flash limits, being therefore detectable by the field amplification. Longer duration of the flash ionization process would also mean better chance of detecting the response signal under the same time resolution of detection. Thus, high time resolution of detection would be sufficient for detecting highly amplified pulse response of the field from 'intermediate' conductivity time flash, while both high time resolution and high intensity resolution (and so, high signal-to-noise ratio) are needed to detect stronger flash events.

Powerful flash ionization events like TGFs are expected to produce effects of 'big' flashes, according to the high peak conductivity values as in Fig. 3. They are therefore detectable only by the field's damping. Note that when mentioning 'big' and 'intermediate' flashes of conductivity, we compare the conductivity peak values for the same duration of the conductivity flashes. For the duration being of the order of 10^{-5} s, the boundary between the 'strong' and the 'intermediate' flash events is around the conductivity peak values at few thousand s^{-1}. For longer duration, higher conductivity peak values are required to classify the flash event as 'strong'.

5.3 Temporal variations of the signal

The discussed above signatures of the cyclotron emission transformation by a flash ionization event can be expected in a form shown in Fig. 3 in the case when the emission is observed continuously. Due to high directivity of the cyclotron emission and to the emitting body's rotation, this can only happen if the geometry of rotation allows the radiated beam/cone staying at the same place with respect to the observer, or if the observing station is following the body's (planet's) rotation.

In most of the cases, the emission is seen as periodic bursts at the phases when the beam turns towards Earth (e.g. Hallinan et al. 2007; Doyle et al. 2010), as in Fig. 9 (top). If a flash ionization

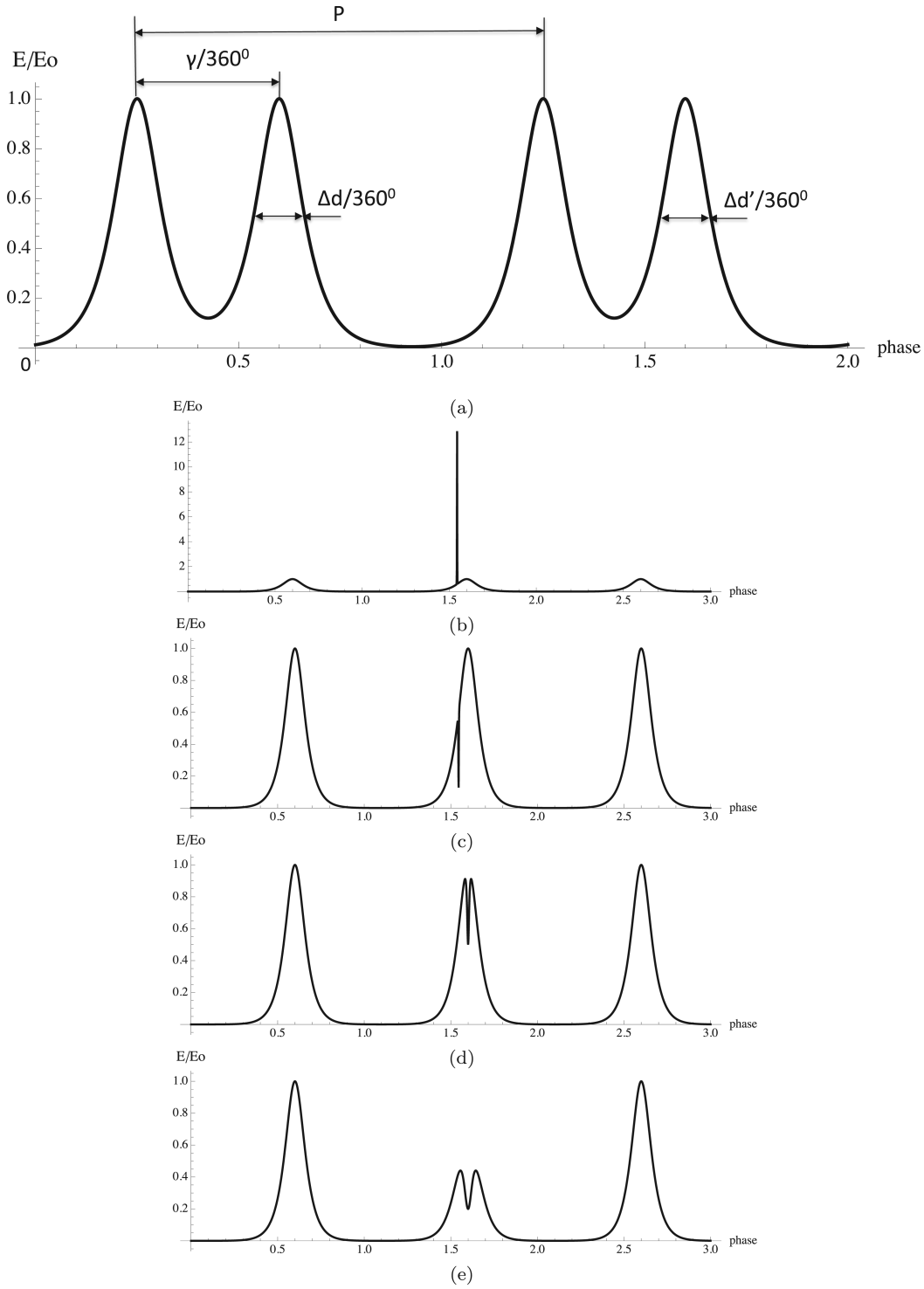

Figure 9. Time evolution of the electric field magnitude, $E(t)$, in units of the magnitude of the unperturbed field, E_0. Top: full two-peaked radio signal from the two cone walls with an observed time delay, $\gamma/360^\circ$ related to the cone opening angle, and a beam width, Δd, which is equivalent to the emission cone wall thickness (compare Fig. 1). The double-peaked signal repeats after a rotational period, P. The unperturbed case is shown where $\Delta d = \Delta d'$. Time-dependent changes in the atmospheres and flash ionizations can cause $\Delta d \neq \Delta d'$ Bottom: examples of a periodically seen cyclotron emission (top) transformed by a flash ionization event as a function of phase. Only the changing amplitudes for one emission beam are shown. Bottom first row: (case (a)) amplification of electric field amplitude through intermediate conductivity flash peak values as in Fig. 4 (top). Bottom second–fourth rows: (cases b–d): damping of electric field through large conductivity flash peak values as in Fig. 4 (bottom).

Table 1. Flash parameters for example cases of cyclotron emission changes due to flash ionization encounter. These numbers are to visualize the effect and will change for more realistic beam functions, multi-dimensional scattering effects, etc. The flash duration $\Delta\sigma$ is taken at FWHH.

Cases in Fig. 9:	a	b	c	d
Flash parameters (equation 20):				
A	2.50×10^{12}	2.50×10^{13}	3.50×10^{13}	4.00×10^{13}
B	1.44×10^{2}	1.44×10^{2}	2.304×10^{3}	2.304×10^{3}
C	3.00×10^{9}	3.00×10^{10}	4.00×10^{10}	4.50×10^{10}
D	-1.44	-1.44	-23.04	-23.04
b	8.33×10^{-1}	8.33×10^{-1}	2.083×10^{-1}	2.083×10^{-1}
k	2.0	2.0	2.0	2.0
Flash properties:				
Duration $\Delta\sigma$ (s)	30	30	120	120
Peak value σ_{max} (s^{-1})	5×10^{11}	5×10^{12}	7×10^{12}	8×10^{12}
	Intermediate	Large	Large	Large
	Flash	Flash	Flash	Flash
Electric field response (Fig. 9):				
	Amplified	Damped	Damped	Damped

event happens on the path of one of the periodic beams (Fig. 1) out of the atmosphere, it would not change the periodicity but influence the signal's amplitude.

Fig. 9 visualizes four example cases how flash ionization can alter a cyclotron signal. The beam shapes were calculated from $E(t)/E_0 = \mathrm{sech}[10\ (2t - 1)] + \mathrm{sech}[10\ (2t - 3)] + \mathrm{sech}[10\ (2t - 5)]$ ($\mathrm{sech}(t) = (\cosh(t))^{-1}$, t – time in units of phase) but any suitable function (like Gaussian) could be used. Please note that the plots in Fig. 9 do not include rigorous modelling of the propagation of the transformed (by flash ionization) signal towards the observer. Instead, a model modulation function (imitating effects of the emission source's rotation) shown in Fig. 9(a) is used. The plots in Figs 9(b)–(d) are obtained as products of the field transformed by the transient event and the modulation function. In this way, the plots represent predictions for the observations, while plots in Fig. 4 present the transformed field at the source. The top panel in Fig. 9 summarizes the ideal, unperturbed situation where two emission beams reoccur after one rotational period, P. The half-height width of the peaks is determined by the wall thickness, Δd, of the emission cone as shown in Fig. 1. The time interval between the two beams, i.e. between the emission maxima, is related to the emission cone opening angle, γ (Fig. 1). The changing peak height and width of the cyclotron emission due to an encounter with a lighting flash, for example, are shown in the second and third rows in Fig. 9. These figures result from solving equations (17) and (18) for the electric field component applying a parametrized conductivity function (equation 20, see also Section 3.3). The necessary parameters for the presented results are summarized in Table 1.

Depending on the peak value of the conductivity flash induced by the ionization and on its duration, the field modulation by the flash is either a short powerful burst of radiation [sharp increase of the amplitude, as in Fig. 9, case (a)], or a damping of the whole radiation peak [Fig. 5, cases (c) and (d)], or its fragment [Fig. 9, case (b)]. The transformation of cyclotron emission which is seen in observations of JO746+20 in Route (2013, their fig. 5.01) looks similar to shown in Fig. 9 and can potentially be a sign of flash ionization events affecting the cyclotron emission.

Detecting a signal pattern as shown in Fig. 9 can be indicative of flash ionization events in the object's atmosphere and magnetosphere (like lightning or TGF). The cyclotron emission is produced by an electron beam moving along the star/dwarf/planet's magnetic field lines. Its power depends on the beam's properties, including its geometrical properties, and number density and velocity distributions. Significant amplification of a regularly seen emission, like shown in Figs 9(b) and (c), is unlikely to happen due to sudden changes in the beam, because of unrealistically high amplitude for cyclotron emission. Damping of the whole signal or its fragment, however, could also be caused by the electron beam variations. Simultaneous optical observations can help to exclude or confirm the beam's variations, as visible aurora is induced by the same beam as the radio cyclotron emission. Variations seen in the visual aurora's geometrical pattern and intensity are expected to correlate with variations in radio emission from the same beam. The radio waves refract differently compared to optical waves; hence, radio waves will travel through different part of the atmosphere than optical waves. Therefore, if the radio waves pass through a localized flash ionization event, the optical light may miss it. In a situation when the visible light is still affected by the same event, this effect should be smaller than that for radio emission, because the visible light is emitted and propagates in a thicker cone. Therefore, the observed visible signal is an integral effect of the light emerging from a significantly larger external surface of the atmosphere than that of a directed radio cyclotron beam. In this way, only a small portion of this visible light can be affected by a local event, making the effect of flash ionization on visible light smaller compared to its effect on radio waves.

Another reason for cyclotron emission variability is spin modulation of the emission due to a character of the star/planet's rotation. In particular, when a planet's magnetic dipole is offset from its rotation axis, the solar/star wind electrons at different rotation phase have different paths towards the magnetic poles. This results in the emission produced at different altitudes, where different values of magnetic field account for the emission variability (Morioka et al. 2013).

5.4 Time-scale of the field response

The duration of the response field pulse (including both cases of amplification and damping in the pre-existing radiation waveform) is determined by duration, $\Delta\sigma$, of the conductivity flash. As discussed in Section 3.4, for the single discharges in Earth atmosphere, the response field pulse is about 10 times shorter than the duration of the

discharge. For Saturn it was found that it is only five times shorter (Farrell et al. 1999). Though single branches of lightning in Earth atmosphere are known to last for a few μs to a few ms, a lightning event consists of a tree of strokes, coming as groups of branches. Pawar & Kamra (2004), studying multiple-discharge flashes in the atmosphere of Earth, found that flashes in each group are bunched together for 15–20 min. There are also reasons to expect longer discharges in extraterrestrial atmospheres with different compositions and higher local pressure. The duration of discharges in air is limited by electron attachment because free electrons are easily lost in air through attachment to oxygen. Duration of discharges in other gases and under higher-than-Earth atmospheric pressure can be significantly longer than in air, as proved by experiments in Briels et al. (2008). The field's response stretches in time proportionally to the longer integral flash duration, reaching about 5–10 folds of the flash's duration, which makes it observable with current instrumentation for large/average expected flashes of lightning. A time resolution on a scale shorter than the response pulse duration is needed to follow the shape of the response filed pulse (waveform). However, for its detection, even one measurement within its duration will be indicative (Fig. 9, lower panels) which can be obtained even when the resolution is lower than the response duration. This makes the detectability subject to the statistical occurrence of transient ionization events which is well studied on Earth, and to a lesser extent for the Solar system planets. From Fig. 9 one also concludes that for an example period of $P \approx 4$ h, a large flash would cause a substantial damping of the emission peak by ≈50 per cent with a time dip of ≈3.2 min (case (d) in Fig. 9). Intermediate flashes do produce a substantial amplification over a very short time window (case (a) in Fig. 9).

5.5 Recipes for observations

We have shown that transient ionization events can leave an imprint on radiation that intercepts a time-dependent ionized gas, like an atmosphere affected by lightning discharges. In the case of BDs, cyclotron maser emission is a good candidate for the 'probe signal'. Observing the cyclotron periodic bursts for several rotational periods (not necessarily consequent) is needed to spot a variability. To interpret it as a signature of a flash ionization event which happened at a location along the cyclotron signal's path, we suggest the following analysis of the detected varied electromagnetic field.

(i) Several orders of magnitude's flash amplification of the initial signal, on a time-scale comparable to the cyclotron radio emission wave period, is a strong indication of a flash ionization event. The detection of such amplitude amplification of the cyclotron emission (or any other signal carrier) requires a high time resolution. The amplification seen in observations [Fig. 4(a) for continuous emission, and Figs 9(b) and (c) for periodically seen emission] suggests an 'intermediate' peak value of the conductivity flash produced by the ionization being the cause.

(ii) Flash (e.g. brief, short term, on a time-scale comparable to the cyclotron emission wave period) damping of the observed radio signal [Fig. 4(b) for continuous emission, and Figs 9(c)–(e) for periodically seen emission] can be a signature of a strong flash ionization. It can though be confused with effects of beam variations and with spin modulation of the cyclotron emission due to the source's rotation.

(iii) Simultaneous observations in optical wavelength can help to distinguish the damping effect of the flash ionization from effects of the beam variations (i.e. variations in the beam of electrons producing both optical aurora and radio emission). If there is no correlation between the radio variability and the variability in the optical aurora, the influence of beam variations can be ruled out as both radio and optical emissions are produced by the same beam of electrons.

(iv) Spin modulation of the cyclotron radio emission due to the source's rotation (Morioka et al. 2013) can be ruled out or subtracted from the observations if observing the object for several consequent periods of rotation.

(v) BDs are thought to have turbulent atmospheres, as concluded from variability measurements and cloud detections (Helling & Casewell (2014)), e.g. variability seen in Luhman 16B (Luhman 2012; Gillon et al. 2013; Burgasser et al. 2014). The turbulent atmospheres have a higher rate of transient flash ionization events like discharges or explosions, as seen for Saturn (Fischer et al. 2011). Some of BDs known for radio cyclotron emission are also fast rotators, e.g. TVLM513 has a period of just 1.9673 h (Hallinan et al. 2007; Doyle et al. 2010). This makes them easier objects for multi-period observations.

6 SUMMARY OF IMPLICATIONS

The motivation behind this research is to find a way to probe atmospheric discharge processes which are otherwise inaccessible. For this purposes, we investigated if and how a coherent emission (e.g. a cyclotron maser radio emission) could be modulated by passing through a region with flash ionization processes in, for example, an atmospheric environment or a magnetosphere. Our results are applicable to a wider variety of problems in astrophysics when a pre-existing radiation travels through a rapidly ionizing medium. These can include discharges in protoplanetary discs (Muranushi, Okuzumi & Inutsuka 2012) and possibly fast radio bursts [see e.g. Thornton et al. (2013) which could be attributed to flash transient events if their variations are not periodically detected].[13] Our model (equations 17–19) can also be applied to microwave background changed during the reionization epoch (Loeb 2002) if the limitations of 1D space-uniform consideration are reasonable for a particular scenario.

We develop a model to describe the influence of flash ionization events on pre-existing radiation that passes through the region where the transient events happen. We solved a (direct) problem of electromagnetic field transformation as a result of the flash transient events and provide a recipe for observers in Section 5.5. Our main conclusions are as follows.

(i) The transformation of coherent emission by fast transient processes in the medium of its propagation can be observable.

(ii) Attributing larger signal perturbations to more powerful processes is not always correct, as more powerful processes can lead to smaller response signals.

(iii) Flash processes of intermediate intensity can be detected by short-term amplification of the signal. The response field's duration can be related to the flash ionization's time-scale and intensity (Fig. 6).

(iv) If the initial emission signal is powerful enough to detect the character of the damping, the small pulse's amplitude and duration in the response field can provide information about the ionization flash magnitude (peak value of conductivity) and duration.

[13] In the opposite case, when periodical field flashes are detected, those are more likely to be attributed to planets or stars companions to a pulsar (Thornton et al. 2013).

(v) If the detection of the field's variation is possible for several related flashes (attributed to the same undergoing event, like multiple strokes of the same cloud-to-ground lightning discharge) and allows deriving the conductivity peak values from additional information, it would be possible to determine whether the discharges started as runaway electrons break down or rather like capacity discharges, by deriving the dependence of the field responses' maximum values on maximum value of the conductivity change. The absence of a noticeable plateau in this dependence (see Fig. 5) suggests that the runaway breakdown discharge is likely to be a source of the ionization, which requires about 10 times lower voltage to enable the discharge in comparison to a conventional capacity-like discharge. If the plateau is noticeable, then a capacitor-like discharge is more probable.

ACKNOWLEDGEMENTS

We gratefully acknowledge the support from the European Community under the FP7 by the ERC starting grant 257431 and are thankful for computer support from the University of St Andrews, SUPA School of Physics & Astronomy. Majority of reference search was done with the help of ADS which is appreciated. We also thank Paul Rimmer for reading and commenting on our manuscript.

REFERENCES

Aleksandrov N. L., Bazelyan E. M., 1999, Plasma Sources Sci. Technol., 8, 285
Apai D., Radigan J., Buenzli E., Burrows A., Reid I. N., Jayawardhana R., 2013, ApJ, 768, 121
Bailey R., Helling C., Hodasan G., Stark C. R., 2013, ApJ, 784, 43
Berger E. et al., 2010, ApJ, 709, 332
Bickerton R. J., 1958, Proc. Phys. Soc., 72, 618
Bingham R., Cairns R. A., Kellett B. J., 2001, A&A, 370, 1000
Bingham R. et al., 2013, Space Sci. Rev., 178, 695
Briels T. M. P., Veldhuizen E. M., van and Ebert U. M., 2008, J. Phys. D: Appl. Phys., 41, 23
Bruce C. E. R., Golde R. H., 1941, J. IEE, 88, 487
Buenzli E. et al., 2012, ApJ, 760, L31
Burgasser A. J., Melis C., Zauderer B. A., Berger E., 2013, ApJ, 762, L3
Burgasser A. J. et al., 2014, ApJ, 785, 48
Cairns R. A., Vorgul I., Bingham R., 2008, Phys. Rev. Lett., 101, 21
Carlson B. E., Lehtinen N. G., Inan U. S., 2010, J. Geophys. Res., 115, A10324
Casewell S. L. et al., 2015, MNRAS, 447, 3218
Cook B. A., Williams P. K. G., Berger E., 2014, ApJ, 785, 1
Crossfield I. J. M. et al., 2014, Nature, 505, 654
de Pater I., Lissauer J. J., 2010, Planetary Sciences. Cambridge Univ. Press, Cambridge
Doyle J. G., Antonova A., Marsh M. S., Hallinan G., Yu S., Golden A., 2010, A&A, 524, A15
Dwyer J., Smith D., Cummer S., 2012, Space Sci. Rev., 173, 133
Ergun R. E., Carlson C. W., McFadden J. P., Delory G. T., Strangeway R. J., Pritchett P. L., 2000, ApJ, 538, 456
Farrell W. M., Kaiser M. L., Desch M. D., 1999, Geophys. Res. Lett., 26, 2601
Farrell W. M., Kaiser M. L., Fischer G., Zarka P., Kurth W. S., Gurnett D. A., 2007, Geophys. Res. Lett., 34, 6202
Fischer G. et al., 2011, Nature, 475, 75
Fishman G. J. et al., 1994, Science, 264, 1313
Gardner R. L., Frese M. H., Gilbert J. L., Longmire C. L., 1984, Phys. Fluids, 27, 2694
Gillon M., Triaud A. H. M. J., Jehin E., Delrez L., Opitom C., Magain P., Lendl M., Queloz D., 2013, A&A, 555, L5
Gurevich A. V., Karashtin A. N., 2013, Phys. Rev. Lett., 110, 185005
Gurevich A. V., Valdivia J. A., Milikh G. M., Papadopolous K., 1996, Radio Sci., 31, 6
Hallinan G. et al., 2007, ApJ, 663, L25
Hallinan G., Antonova A., Doyle J. G., Bourke S., Lane C., Golden A., 2008, ApJ, 684, 644
Heinze A. N. et al., 2013, ApJ, 767, 173
Helling C., Casewell S., 2014, A&AR, 22, 0935
Helling C., Jardine M., Mokler F., 2011, ApJ, 737, 38
Helling C., Jardine M., Stark C., Diver D. A., 2013, ApJ, 767, 136
Imai K., Riihimaa J. J., Reyes F., Carr T. D., 2002, J. Geophys. Res., 107, 1081
Kellett B. J., Graffagnino V., Bingham R., Muxlow T. W. B., Gunn A. G., 2007, preprint (astro-ph/0701214)
Khizhnyak N. A., 1986, Integral Equations of Macroscopic Electrodynamics. Naukova Dumka, Kiev
Kramer M., Wielebinski R., Jessner A., Gil J. A., Seiradakis J. H., 1994, A&AS, 107, 515
Kuznetsov A., Doyle J., Yu S., Hallinan G., Antonova A., Golden A., 2012, ApJ, 746, 99
Lamy L. et al., 2010, Geophys. Res. Lett., 37, 12104
Lo K. K. et al., 2012, MNRAS, 421, 3316
Loeb A., 2002, in Gilfanov M., Sunyaev R., Churazov E., Lighthouses of the Universe: The Most Luminous Celestial Objects and Their Use for Cosmology. Springer-Verlag, Berlin, p. 137
Lu G. et al., 2010, Geophys. Res. Lett., 37, L11806
Lu G., Cummer S. A., Li J., Han F., Smith D. M., Grefenstette Brian W., 2011, J. Geophys. Res.: Space Phys., 116, A03316
Luhman K. L., 2012, ARA&A, 50, 65
Luque A., Ebert U., 2013, New J. Phys., 16, 013039
Lynch C., Mutel R. L., Güdel M., 2015, ApJ, 802, 106
McConville S. L. et al., 2008, Plasma Phys. Control. Fusion, 50, 074010
MacLachlan C. S., Diver D. A., Potts H. E., 2009, New J. Phys., 11, 063001
Marisaldi M. et al., 2013, J. Geophys. Res.: Space Phys., 119, 1337
Metchev S. et al., 2013, Astron. Nachr., 334, 40
Miller S. L., Urey H. C., 1959, Science, 131, 3370
Morioka A., Miyoshi Y., Kurita S., Kasaba Y., Angelopoulos V., Misawa H., Kojima H., McFadden J. P., 2013, J. Geophys. Res.: Space Phys., 118, 1123
Muranushi T., Okuzumi S., Inutsuka S.-I., 2012, ApJ, 760, 56
Mutel R. L., Christopher I. W., Pickett J. S., 2008, Geophys. Res. Lett., 35, L07104
Nerukh A. G., Sakhnenko N., Benson T., Sewell P., 2012, Non-Stationary Electromagnetics. Pan Stanford Publ, Singapore.
Østgaard N., Gjesteland T., Carlson B. E., Collier A. B., Cummer S. A., Lu G., Christian H. J., 2013, Geophys. Res. Lett., 40, 2423
Pawar S. D., Kamra A. K., 2004, J. Geophys. Res.: Atmos., 109, D02205
Radigan J., Jayawardhana R., Lafrenière D., Artigau E., Marley M., Saumon D., 2012, ApJ, 750, 105
Rakov V. A., Uman M. A., 2003, Lightning. Cambridge Univ. Press, Cambridge
Rakov V. A., Uman M. A., 2007, Lightning: Physics and Effects. Cambridge Univ. Press, Cambridge
Rimmer P., Helling C., 2013, AJ, 774, 108
Rodrigues-Barrera I., Helling C., Stark C., Rice A., 2015, MNRAS, 454, 3977
Route M. P., 2013, PhD thesis, The Pennsylvania State University
Rycroft M. J., 2006, Introduction to the Physics of Sprites, Elves and Intense Lightning Discharges, in NATO Sci Series II: Math, Phys and Chem., 225, Sprites, Elves and I tense Lightning Discharges, p. 1
Sanghvi J. R., 2008, Int. J. Energy Environ., 2, 16
Schellart P. et al., 2015, Phys. Rev. Lett., 114, 165001
Schrijver C. J., 2009, ApJ, 699, L148
Siingh D., Singh A. K., Patel R. P., Singh R., Singh R. P., Veenadhari B., Mukherjee M., , 2008, Surv. Geophys., 29, 499
Skordoulis C., Sarantopoulou E., Spyrou S., Cefalas A., 1990, J. Mod. Opt., 37, 501
Speirs D. C., McConville S. L., Gillespie K. M., Phelps A. D. R., Ronald K., Ronald, 2013, J. Plasma Phys., 79, 999

Stark C. R., Helling Ch., Diver D. A., Rimmer P. B., 2013, ApJ, 766, 11
Thornton D. et al., 2013, Science, 341, 53
Trigilio C., Leto P., Umana G., Buemi C. S., Leone F., 2008, MNRAS, 384, 1437
Tsalkou Y. A., Tikhomirov V. V., Marozava H. P., 2013, preprint (arXiv:1301.5506)
Uman M. J., 1964, Atmos. Terr. Phys., 26, 2
Vorgul I., 2007, Phil. Trans. R. Soc. A, 366, 1871
Vorgul I. et al., 2011, Phys. Plasmas, 18, 5
Wang L., Carr T. D., 1995, J. Geophys. Res., 100, 21669
Williams P. K. G., Cook B. A., Berger E., 2014, ApJ, 785, 9
Williams P. K. G., Berger E., Irwin J., Berta-Thompson Z. K., Charbonneau D., 2015, ApJ, 799, 192
Yu S., Doyle J. G., Kuznetsov A., Hallinan G., Antonova A., MacKinnon A. L., Golden A., 2012, AJ, 752, 60
Zarka P., Farrell W., Fischer G., Konovalenko A., 2008, Space Sci. Rev., 137, 257
Zhang X., Showman A. P., 2014, ApJ, 788, L6

This paper has been typeset from a TEX/LATEX file prepared by the author.